Excellent thermoelectric performance of boron-doped n-type Mg₃Sb₂-based materials *via* the manipulation of grain boundary scattering and control of Mg content

Xiaoxi Chen[1†], Jianbo Zhu[1†], Dandan Qin[1], Nuo Qu[1], Wenhua Xue[2], Yumei Wang[2], Qian Zhang[3], Wei Cai[1], Fengkai Guo[1*] and Jiehe Sui[1*]

ABSTRACT   Thermoelectric devices require thermoelectric materials with high figure-of-merit (ZT) values in the operating temperature range. In recent years, the Zintl phase compound, n-Mg_3Sb_2, has received much attention owing to its rich chemistry and structural complexity. However, it hardly achieves high ZT values throughout the medium temperature range. Herein, by increasing the sintering temperature as much as possible, we successfully increased the average grain size of the compound by 15 times, and the grain boundary scattering was manipulated to obtain high carrier mobility of up to 180 cm^2 V^{-1} s^{-1}. Simultaneously, we optimized the Mg content for ultralow lattice thermal conductivity. We first doped the Mg_3Sb_2-based materials with boron for higher sintering temperature, good thermal stability, and higher hardness. The synergistic optimization of electrical and thermal transport resulted in excellent ZT values (0.62 at 300 K, 1.81 at 773 K) and an average ZT of 1.4 (from 300 to 773 K), which are higher than the state-of-the-art values for n-type thermoelectric materials, demonstrating a high potential in device applications.

Keywords: grain boundary scattering, boron doping, excess Mg, Mg_3Sb_2-based thermoelectrics

INTRODUCTION

Thermoelectric devices, which enable direct conversion between heat and electricity, have always been associated with energy crisis [1–4]. They can be employed in a wide range of application scenarios, such as power supply for internet of things (IoT) devices [5], refrigeration [6–11], waste heat recovery [12], and radioisotope thermoelectric generators [13–15]. These multiplex devices require excellent thermoelectric performance over the entire temperature range. The conversion efficiency is determined by the materials' thermoelectric figure-of-merit (ZT), expressed as $ZT = S^2\sigma T/\kappa$, where σ, S, κ, and T are the electrical conductivity, Seebeck coefficient, thermal conductivity, and absolute temperature, respectively [16–18]. High thermoelectric performance can be achieved with a good balance among these parameters, which correlate and influence each other through carrier concentration. The optimal carrier concentration can be preliminarily judged by the S range [19]. Advanced strategies are implemented to manipulate the thermoelectric properties, including enhancing the power factor (e.g., modulation doping [20], band engineering [21,22], and Rashba effect [23]) and reducing the lattice thermal conductivity (e.g., point defects [24], dislocations [25], superlattice precipitates [26], and phonon dispersion modulation [27]).

At present, only a few types of thermoelectric materials have been commercialized [28–31]. Therefore, there is a need for novel thermoelectric materials with wide temperature range and high thermoelectric performance. To realize thermoelectric materials with wider operating temperature ranges, wide bandgaps, layered structures, and low-symmetry crystal structures are desired [32]. Recently, n-type Mg_3Sb_2, which is an intrinsic p-type Zintl compound [33–36], was synthesized by Tamaki *et*

al. [37] with a relatively high ZT (~1.5) at 773 K. Since then, many efforts have been made to improve its performance. The exceptionally high ZT of the n-type Mg_3Sb_2 is attributed to the multiple-valley conduction bands [38–40] and its intrinsically low lattice thermal conductivity [41,42]. Some of the strategies employed include manipulating the carrier scattering mechanism [43–45], defect chemistry [46,47], band engineering [40,48,49], and grain boundary scattering [49–54]. The n-type Mg_3Sb_2-based materials have achieved peak ZT of over 1.8 at 773 K by doping on the Mg2 sites with dopants such as Mn [45], Co [43] and Nb [44]. However, the room-temperature ZT of these samples are relatively low (< 0.4) due to the ionized impurity scattering in low-temperature ranges. To enhance the room-temperature ZT, coarse grains of over 30 μm have been designed by alloying with elements with low melting points (Mg_3Bi_2 [48,49]) or *via* melting [52,53]/annealing [54] methods, which require tantalum-sealing technique or a specially designed Mg-vapor annealing system. The ZT value has been greatly enhanced to about 0.8 at 300 K, but the peak ZT is sacrificed to an extent at the same time. Currently, balancing both room-temperature and high-temperature performance of Mg_3Sb_2-based materials is a challenge. Because the average ZT value is pivotal in thermoelectric devices [55–57], obtaining high ZT values in a wide temperature range has attracted a lot of attention.

For n-type Mg_3Sb_2-based materials, low carrier mobility in low-temperature ranges is vital to further improve their low-temperature performance [43,46]. One of the reasons is that the ionized impurity scattering is a result of the presence of intrinsic Mg vacancies [37,47]. The intrinsic Mg vacancies could easily become negatively charged, which is the main cause of the ionized impurity scattering, resulting in poor carrier mobility. Another reason is that the ionized impurity scattering originates from the grain boundary scattering and could be suppressed by increasing the grain size [51,58]. Recently, Imasato et al. [59] prepared the single-crystal n-type Mg_3Sb_2 with no evidence of ionized impurity scattering, indicating the critical role of grain boundaries on the carrier scattering mechanism and thermoelectric performance of the n-type Mg_3Sb_2-based materials.

In this work, to improve the low-temperature performance of the n-type Mg_3Sb_2-based material, we modulated the grain boundary scattering by simply optimizing the sintering conditions. Much high-temperature sintering was performed to maximize the grain size, thus minimizing the carrier scattering. Boron, which has been proven to have a stabilizing effect [60–62], was first in-

troduced to Mg_3Sb_2 to increase its sintering temperature. For the present experimental condition, without the boron doping, samples sintered at over 1073 K became p-type due to the volatilization of the Mg component, whereas, with the boron doping, good n-type performance was maintained at sintering temperatures as high as 1093 K, which is beneficial to achieving much larger grain sizes and better electrical performance. In addition, it enhances the hardness of Mg_3Sb_2-based materials. Besides, to minimize the lattice thermal conductivity, the excess Mg content due to magnesium volatilization caused by high-temperature sintering, which easily results in high lattice thermal conductivity, was minimized. As a result, by maximizing the sintering temperature, the grain size became larger and the grain boundary scattering was suppressed, achieving better electrical transport characteristics. The Hall mobility was significantly enhanced (from 20 to 180 $cm^2 V^{-1} s^{-1}$), leading to a high power factor of ~24 $\mu W\ cm^{-1}\ K^{-2}$ at 373 K. The lattice thermal conductivity was also reduced dramatically in the entire temperature range mainly due to the minimized excess Mg content. Consequently, excellent ZT values were obtained (0.62 at 300 K, 1.81 at 773 K), which exceed the state-of-the-art value for n-type Mg_3Sb_2-based materials. This work demonstrates the key role of grain boundary scattering and the existence of excess Mg content in further improvement of the thermoelectric performance of n-type Mg_3Sb_2-based materials.

EXPERIMENTAL SECTION

Synthesis
Magnesium turnings (Mg, 99.98%; Alfa Aesar), antimony shots (Sb, 99.8%; Alfa Aesar), bismuth pieces (Bi, 99.99%; Alfa Aesar), tellurium pieces (Te, 99.999%; Alfa Aesar), and boron pieces (B, 99.999%; Alfa Aesar) were weighed according to the composition of $B_{0.03}Mg_{3.17}Sb_{1.5}Bi_{0.49}Te_{0.01}$ in a glove box under an argon atmosphere with oxygen and water levels below 0.5 ppm. They were loaded into a stainless-steel ball-milling jar and milled for 10 h using SPEX 8000M. Thereafter, the ball-milled fine powder was loaded into a graphite die and sintered instantly by spark plasma sintering at 923–1093 K and the pressure of ~50 MPa for 2 min.

Phase and property characterizations
X-ray diffraction (XRD) analysis was performed using a PANalytical multipurpose diffractometer with an X'celerator detector (PANalytical X'Pert Pro). No impurity phase was found in the hot-pressed disk samples within

the detection limit of the XRD spectrometer. Bar samples were cut from the pressed disks and used for both the electrical resistivity (ρ) and S measurements on a commercial system (CTA-3). The thermal conductivity was calculated using the relation $\kappa = DC_p d$, where D, C_p, and d are the thermal diffusivity coefficient, specific heat capacity, and density of the sample, respectively. The D was measured using a laser flash system (Netzsch LFA 457, Germany). The C_p was measured using a differential scanning calorimetry thermal analyzer (Netzsch DSC 404C, Germany). The d was determined by the Archimedes method. The Hall coefficient (R_H) was measured using a Physical-Property Measurement System (a homemade instrument). The Hall carrier concentration (n_H) was calculated using the expression of $n_H = 1/eR_H$ and the Hall carrier mobility (μ_H) was calculated by $\sigma = e\mu_H n_H$, where e is the electronic charge and σ is the electrical conductivity. The morphology was investigated by scanning electron microscopy (SEM) on FEI Quanta 200FEG. EDS was performed using a JEOL ARM200F atomic resolution analytical electron microscope.

RESULTS AND DISCUSSION

Fig. 1a shows the XRD patterns of the $Mg_{3.17}B_{0.03}Sb_{1.5}Bi_{0.49}Te_{0.01}$ samples sintered at different temperatures (923, 1023, 1073, and 1093 K). All the main diffraction peaks are well indexed to the α-Mg_3Sb_2 phase with the inverse α-La_2O_3 structure (space group $P\bar{3}m1$), and no obvious secondary phase is observed. The lattice parameters decreased with increasing sintering temperature, as shown in Fig. 1b. Increasing the sintering temperature, which causes more Mg content to volatilize, resulted in an increase in the number of Mg vacancies, leading to slightly decreased lattice parameters.

To verify the change in the Mg content at different sintering temperatures, the compositions of the $Mg_{3.17}B_{0.03}Sb_{1.5}Bi_{0.49}Te_{0.01}$ samples were analyzed by energy-dis-

persive X-ray spectroscopy (EDS) and listed in Table 1. As the sintering temperature increased from 923 to 1093 K, the measured Mg content reduced sharply from 3.158 to 3.014 (relative to the Sb amount of 1.5), but no obvious change was observed in the other constituents. Meanwhile, the value of 3.014 is close to the lowest Mg content reported in the literature, which can ensure good performance of the n-type Mg_3Sb_2 materials [63,64], and it is consistent with the transition to p-type material obtained herein when the sintering temperature exceeded 1093 K.

Owing to the greatly increased sintering temperature, the grain size has also remarkably increased, as shown in Fig. 2. The obtained grain size distribution is shown in Fig. S1. When the sample was sintered at 923 K, the average grain size was about 1 μm, which increased to 16 μm (more than 15 times) when the sintering temperature increased to 1093 K. Such a large average grain size is in the same order of magnitude as that of the samples prepared *via* melting and annealing methods (~30 μm) in the previous reports [53,54]. The large grains observed in the sample sintered at higher temperatures indicate the reduction of the grain boundary density and the attenuation of the grain boundary scattering, leading to enhanced carrier mobility and, in turn, improved electrical performance. This will be further discussed in the later section. The accumulated lattice thermal conductivity of $Mg_3Sb_{1.5}Bi_{0.5}$ as a function of the phonon free mean path saturates around 2 μm at room temperature [50], and thus the thermal conductivity is little affected by grain growth when the grain size is larger than 2 μm.

The potential barriers at the boundaries have a strong scattering effect on the carrier transport in Mg_3Sb_2 when the temperature is lower than 500 K [50,51], thereby resulting in low carrier mobility. Therefore, the coarse grains obtained herein could reduce the grain boundary density and the scattering of the carriers. Consequently,
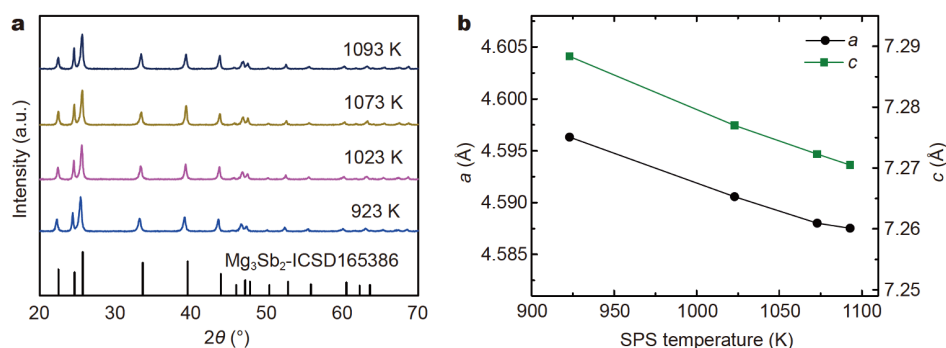

Figure 1 (a) XRD patterns and (b) lattice parameters of $Mg_{3.17}B_{0.03}Sb_{1.5}Bi_{0.49}Te_{0.01}$ specimens sintered at different temperatures.

Table 1 The measured composition of the $Mg_{3.17}B_{0.03}Sb_{1.5}Bi_{0.49}Te_{0.01}$ samples sintered at different temperatures[a]

| Element	923 K	1023 K	1073 K	1093 K
Mg	3.158	3.069	3.030	3.014
Sb	1.500	1.500	1.500	1.500
Bi	0.498	0.504	0.534	0.500
Te	0.015	0.015	0.026	0.023
B	0.043	0.037	0.052	0.049

a) To facilitate comparison, each element composition is converted based on the fixed Sb amount of 1.5.

the Hall mobility, especially in the low-temperature range, was greatly improved by modulating the grain boundary scattering (Fig. 3a). As shown in Fig. 3c, the room-temperature Hall mobility was increased from ~35 to 180 $cm^2 V^{-1} s^{-1}$ (over fourfold) as the sintering temperature increased from 923 to 1093 K. The carrier concentration showed a slight downward trend with increasing sintering temperature, as shown in Fig. 3b. In the n-type Mg_3Sb_2, Mg vacancies are easily negatively charged and the carrier concentration decreases [63,64]. Excess Mg can suppress the Mg vacancies, thus maintaining good n-type characteristics [37,43,47]. Within a certain range, the carrier concentration is very sensitive to excess Mg. Particularly, the change in Hall concentration,
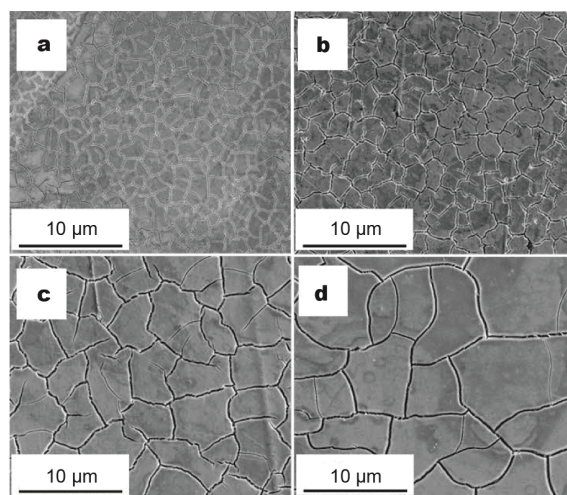
Figure 2 SEM images of $Mg_{3.17}B_{0.03}Sb_{1.5}Bi_{0.49}Te_{0.01}$ of the polished and etched surfaces of the specimens sintered at (a) 923 K, (b) 1023 K, (c) 1073 K, and (d) 1093 K.

as shown in Fig. 3b, is quite consistent with the change in the Mg content in Table 1.

Due to the significantly improved Hall mobility at higher sintering temperatures, the electrical conductivity of the $Mg_{3.17}B_{0.03}Sb_{1.5}Bi_{0.49}Te_{0.01}$ samples was remarkably increased, even though the Hall concentration decreased
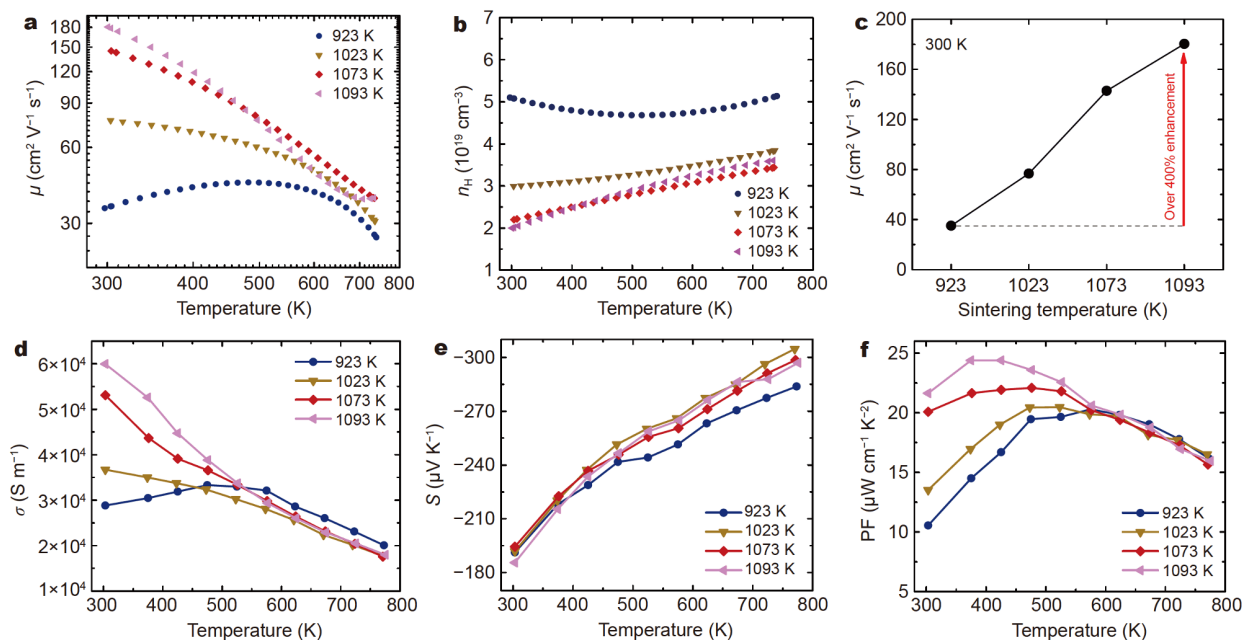

Figure 3 Electrical transport properties of $Mg_{3.17}B_{0.03}Sb_{1.5}Bi_{0.49}Te_{0.01}$ samples sintered at different temperatures. (a) Temperature-dependent Hall carrier concentration and (b) Hall carrier mobility. (c) Room-temperature Hall mobility *versus* sintering temperature. Temperature-dependent (d) electrical conductivity, (e) Seebeck coefficient, and (f) power factor (PF).

slightly, especially in the low-temperature range (Fig. 3d). At temperatures below 500 K, the electrical conductivity increased linearly with the increase in the sintering temperature, reaching 6×10^4 S m^{-1} at room temperature for the sample sintered at 1093 K, which is twice that of the sample sintered at 923 K. In the high-temperature range, the electrical conductivities of all the samples were quite close and the carrier scattering mechanism was dominated by the same phonon scattering. Fig. 3e shows the temperature-dependent S of the $Mg_{3.17}B_{0.03}Sb_{1.5}Bi_{0.49}$-$Te_{0.01}$ samples sintered at different temperatures. The S slightly increased with increasing sintering temperature, which is attributed to the corresponding decrease in the Hall concentration shown in Fig. 3b.

With the remarkably enhanced electrical conductivity and the slightly increased S, the power factors of the samples sintered at higher temperatures were markedly improved (Fig. 3f). The room-temperature power factor was 10.5 µW cm^{-1} K^{-2} for the sample sintered at 923 K and over 21 µW cm^{-1} K^{-2} for that sintered at 1093 K. The peak power factor of 24 µW cm^{-1} K^{-2} was attained at 373 K, which is higher than the state-of-the-art value for n-type Mg_3Sb_2-based materials. The power factor plays an important role in the maximum output power density in thermoelectric devices [65,66], hence, it is meaningful for n-type Mg_3Sb_2 materials to achieve such a high power density at such low temperatures, making them suitable for near room-temperature applications.

The excess Mg content is an important factor that affects the thermoelectric properties of the n-type Mg_3Sb_2. The additional amount of Mg content above the threshold would exist as a second phase, which was confirmed by the EDX-scanning transmission electron microscopy (STEM) mapping, as shown in Fig. 4. A similar phenomenon was reported by Shuai et al. [64]. Such an elemental Mg impurity with a much higher thermal conductivity than Mg_3Sb_2 would increase the thermal conductivity of the sample, and the degree of increase is proportional to the volume fraction of the Mg impurity [63,67]. Such damage to the thermoelectric performance due to excess Mg content was also reported by Shuai et al. [64] and Imasato et al. [63]. In this work, while the grain boundary scattering was modulated, the actual composition of the excess Mg in the material was also optimized via Mg volatilization at different sintering temperatures. Owing to the change in the Mg content (Table 1) and the fact that the material turns into p-type when the sintering temperature exceeds 1093 K, we infer that the Mg impurity in the $Mg_{3.17}B_{0.03}Sb_{1.5}Bi_{0.49}Te_{0.01}$ alloy could be minimized at the sintering temperature of 1093 K, which
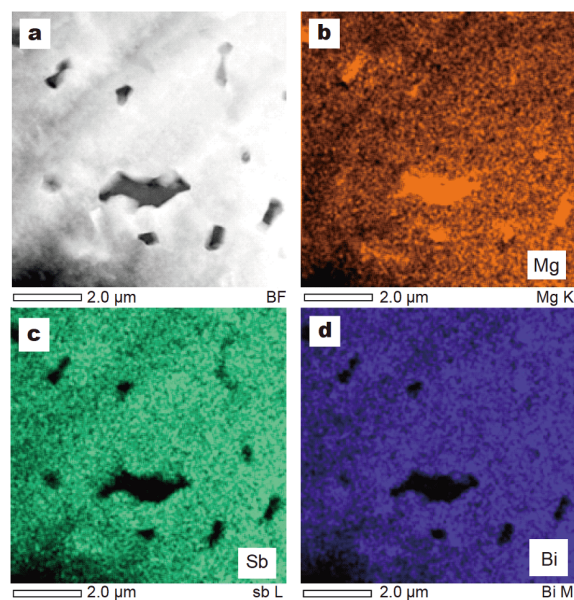

Figure 4 (a) High-angle annular dark field (HADDF)-STEM image and the corresponding EDS mapping of (b) Mg, (c) Sb, and (d) Bi in $Mg_{3.17}B_{0.03}Sb_{1.5}Bi_{0.49}Te_{0.01}$ sample sintered at 1023 K. Mg elemental is confirmed as an impurity.

is conducive to reducing the lattice thermal conductivity. Additionally, as Mg volatilizes more vigorously at high sintering temperatures, the concentration of Mg vacancies also increases, which could also enhance phonon scattering and further reduce the lattice thermal conductivity.

Herein, the total thermal conductivity decreased with increasing sintering temperature, as shown in Fig. 5a; from 1.07 W m^{-1} K^{-1} at room temperature when sintered at 923 K to 0.98 W m^{-1} K^{-1} when sintered at 1093 K. According to the temperature-dependent carrier mobility, the carrier scattering mechanism of the samples sintered at 1073 and 1093 K was dominated by acoustic scattering. Therefore, the Lorenz constant can be determined by a single parabolic band approximation with acoustic scattering. The lattice thermal conductivity (κ_L) can be obtained by subtracting the electrical thermal conductivity κ_{ele} from total thermal conductivity κ_{tot}, and κ_{ele} can be calculated using the Wiedemann-Franz relationship ($\kappa_{ele} = L\sigma T$), as shown in Fig. 5b. The sample sintered at 1093 K exhibited the lowest lattice thermal conductivity of 0.42 W m^{-1} K^{-1} at 773 K, which could be attributed to the ultimate control of the excess Mg and the concomitant increase in the Mg vacancy concentration.

The significantly improved electrical performance obtained by tuning the grain boundary scattering and the simultaneously decreased lattice thermal conductivity due
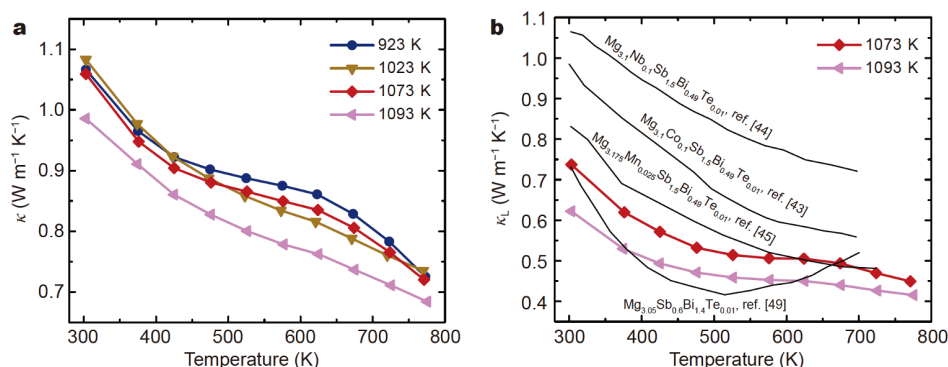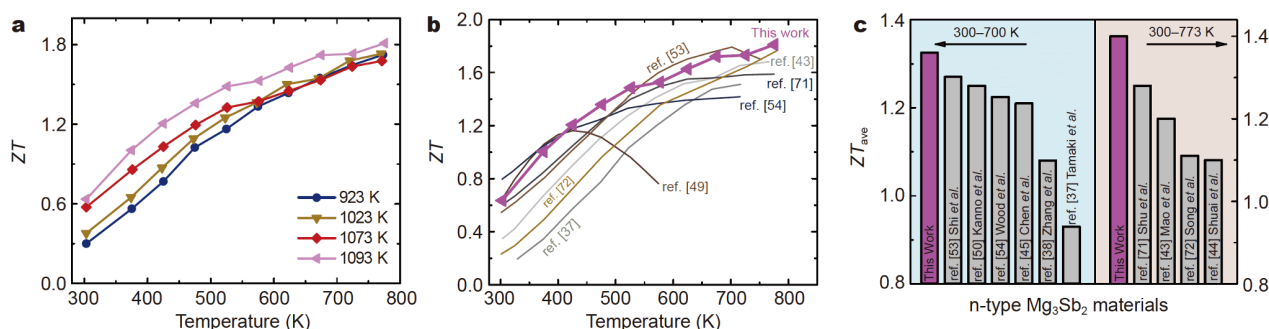
Figure 5 Temperature-dependent (a) total thermal conductivity and (b) lattice thermal conductivity of the $Mg_{3.17}B_{0.03}Sb_{1.5}Bi_{0.49}Te_{0.01}$ samples sintered at different temperatures, compared with other n-Mg_3Sb_2 in the literatures [43–45,49].

to the ultimate control of excess Mg content resulted in a tremendous increase in *ZT* over the entire temperature range, as shown in Fig. 6a. The *ZT* value gradually increased with the sintering temperature, and the $Mg_{3.17}B_{0.03}Sb_{1.5}Bi_{0.49}Te_{0.01}$ sample sintered at 1093 K exhibited both high room-temperature *ZT* of 0.62 and high peak *ZT* of 1.81 at 773 K. Owing to the maximized sintering temperature and the doping effect of boron, the $Mg_{3.17}B_{0.03}Sb_{1.5}Bi_{0.49}Te_{0.01}$ sample sintered at 1093 K showed outstanding performance compared with other n-type Mg_3Sb_2-based materials. The temperature-dependent *ZT* of the boron-doped samples was enhanced in the entire temperature range (Fig. 6b). The $Mg_{3.17}B_{0.03}Sb_{1.5}$-$Bi_{0.49}Te_{0.01}$ sample sintered at 1093 K exhibited the highest average *ZT* value among all other n-type Mg_3Sb_2-based materials (Fig. 6c), demonstrating great potential for practical device applications.

It is worth mentioning that boron doping was chosen for the following reasons. First, it can improve the overall thermal stability of the n-type Mg_3Sb_2 materials. For

boron-free samples, when the sintering temperature is over 1073 K, the volatilization of Mg is too much to keep n-type characteristics. For boron-doped samples, the sintering temperature can reach up to 1093 K while the n-type characteristics are maintained, but it turns to p-type if the sintering temperature is further increased. The thermoelectric performance of the $Mg_{3.17}B_{0.03}Sb_{1.5}Bi_{0.49}$-$Te_{0.01}$ sample sintered at 1093 K was examined *via* consecutive heating cycles, as shown in Fig. S2, and good thermal stability was obtained. It was reported that elemental bismuth would be released from the crystal structure after the first thermal cycle in Te-doped $Mg_3Sb_{1.5}Bi_{0.5}$ [68], whereas no such phenomenon was observed in the B-doped samples after the thermal cycles (Fig. S3), which also indicates the stabilizing effect of boron. Second, boron doping could increase the hardness of Mg_3Sb_2 as in SiGe- [69] and Bi_2Te_3- [70] based materials. The Vickers hardness (Fig. S4) shows an evident improvement, revealing the strengthening effect of B doping on the hardness. Third, B doping has the effects of

Figure 6 (a) Temperature-dependent *ZT* of the $Mg_{3.17}B_{0.03}Sb_{1.5}Bi_{0.49}Te_{0.01}$ samples sintered at different temperatures. Comparison of *ZT* (b) and average *ZT* (c) of the sample obtained in this work and those of other high-performance n-type Mg_3Sb_2 materials [37,38,43,44,50,53,54,71,72]. Since the test temperature ranges of the materials in the literature are different, they are divided into two ranges for the comparison of the average *ZT*.

donor doping and reduces the polarity of the Mg–Sb covalent bond (reducing the electronegativity difference between Mg and Sb), which can simultaneously increase the carrier concentration and mobility, thereby improving the conductivity. In addition to the atomic disorder induced by boron doping, which reduces the thermal conductivity, ZT value was promoted, and the detailed data are shown in Fig. S5. The optimized doping amount of boron was 0.03. The ZT values for $Mg_{3.17}B_{0.03}Sb_{1.5}$-$Bi_{0.49}Te_{0.01}$ and the undoped samples sintered at 923 K are compared in Fig. S6, with that of the B-doped sample sintered at 1093 K as a reference. The comparison shows that the thermoelectric performance was greatly improved by the B doping and the combined effect of the enlarged grain size and ultimately controlled Mg content.

CONCLUSIONS

In summary, boron-doped n-type Mg_3Sb_2-based materials were synthesized. By optimizing the sintering temperature, the grain size was increased, weakening the grain boundary scattering and thus, resulting in a high Hall mobility of over $180\ cm^2\ V^{-1}\ s^{-1}$. The precise control of the excess Mg content along with the increasing sintering temperature resulted in ultralow lattice thermal conductivity. Moreover, the B doping showed a stabilizing effect and increased the hardness of the material. By modulating the grain boundary scattering and the ultimate control of the excess Mg content, high ZT values ranging from 0.61 (at room temperature) to 1.81 (773 K) and an average ZT of 1.4 (at 300–773 K) were obtained. The outstanding thermoelectric performance would advance the deviceization of the n-type Mg_3Sb_2-based thermoelectric materials.

1   Champier D. Thermoelectric generators: A review of applications. Energy Convers Manage, 2017, 140: 167–181

2   Liu W, Jie Q, Kim HS, et al. Current progress and future challenges in thermoelectric power generation: From materials to devices. Acta Mater, 2015, 87: 357–376

3   Goldsmid HJ. Thermoelectric Refrigeration. New York: Springer, 2013

4   Chen ZG, Han G, Yang L, et al. Nanostructured thermoelectric materials: Current research and future challenge. Prog Nat Sci-Mater Int, 2012, 22: 535–549

5   Hong M, Chen ZG, Zou J. Fundamental and progress of Bi_2Te_3-based thermoelectric materials. Chin Phys B, 2018, 27: 048403

6   Pietrzyk K, Ohara B, Watson T, et al. Thermoelectric module design strategy for solid-state refrigeration. Energy, 2016, 114: 823–832

7   Salvador JR, Cho JY, Ye Z, et al. Conversion efficiency of skut-

8   DiSalvo FJ. Thermoelectric cooling and power generation. Science, 1999, 285: 703–706

9   LaLonde AD, Pei Y, Wang H, et al. Lead telluride alloy thermoelectrics. Mater Today, 2011, 14: 526–532

10   Enescu D, Virjoghe EO. A review on thermoelectric cooling parameters and performance. Renew Sustain Energy Rev, 2014, 38: 903–916

11   Shi XL, Zou J, Chen ZG. Advanced thermoelectric design: From materials and structures to devices. Chem Rev, 2020, 120: 7399–7515

12   Hussain QE, Brigham DR, Maranville CW. Thermoelectric exhaust heat recovery for hybrid vehicles. SAE Int J Engines, 2009, 2: 1132–1142

13   He J, Tritt TM. Advances in thermoelectric materials research: Looking back and moving forward. Science, 2017, 357: eaak9997

14   O'Brien RC, Ambrosi RM, Bannister NP, et al. Safe radioisotope thermoelectric generators and heat sources for space applications. J Nucl Mater, 2008, 377: 506–521

15   Zhu T, Liu Y, Fu C, et al. Compromise and synergy in high-efficiency thermoelectric materials. Adv Mater, 2017, 29: 1605884

16   Poudel B, Hao Q, Ma Y, et al. High-thermoelectric performance of nanostructured bismuth antimony telluride bulk alloys. Science, 2008, 320: 634–638

17   Tan G, Shi F, Hao S, et al. Non-equilibrium processing leads to record high thermoelectric figure of merit in PbTe-SrTe. Nat Commun, 2016, 7: 12167

18   Mori T. Novel principles and nanostructuring methods for enhanced thermoelectrics. Small, 2017, 13: 1702013

19   Hong M, Lyu W, Wang Y, et al. Establishing the golden range of Seebeck coefficient for maximizing thermoelectric performance. J Am Chem Soc, 2020, 142: 2672–2681

20   Zebarjadi M, Joshi G, Zhu G, et al. Power factor enhancement by modulation doping in bulk nanocomposites. Nano Lett, 2011, 11: 2225–2230

21   Pei Y, LaLonde AD, Wang H, et al. Low effective mass leading to high thermoelectric performance. Energy Environ Sci, 2012, 5: 7963–7969

22   Fu C, Zhu T, Liu Y, et al. Band engineering of high performance p-type FeNbSb based half-Heusler thermoelectric materials for figure of merit $zT > 1$. Energy Environ Sci, 2015, 8: 216–220

23   Hong M, Lyv W, Li M, et al. Rashba effect maximizes thermoelectric performance of GeTe derivatives. Joule, 2020, 4: 2030–2043

24   Fu C, Bai S, Liu Y, et al. Realizing high figure of merit in heavy-band p-type half-Heusler thermoelectric materials. Nat Commun, 2015, 6: 8144

25   Kim HS, Kang SD, Tang Y, et al. Dislocation strain as the mechanism of phonon scattering at grain boundaries. Mater Horiz, 2016, 3: 234–240

26   Hong M, Zheng K, Lyv W, et al. Computer-aided design of high-efficiency GeTe-based thermoelectric devices. Energy Environ Sci, 2020, 13: 1856–1864

27   Hong M, Wang Y, Feng T, et al. Strong phonon-phonon interactions securing extraordinary thermoelectric $Ge_{1-x}Sb_xTe$ with Zn-alloying-induced band alignment. J Am Chem Soc, 2018, 141: 1742–1748

28   Sootsman JR, Chung DY, Kanatzidis MG. New and old concepts in thermoelectric materials. Angew Chem Int Ed, 2009, 48: 8616–8639

terudite-based thermoelectric modules. Phys Chem Chem Phys, 2014, 16: 12510–12520

29 Yang J, Stabler FR. Automotive applications of thermoelectric materials. J Elec Materi, 2009, 38: 1245–1251

30 Goldsmid HJ. Introduction to Thermoelectricity. New York: Springer, 2010

31 Shakouri A. Recent developments in semiconductor thermoelectric physics and materials. Annu Rev Mater Res, 2011, 41: 399–431

32 Xiao Y, Zhao LD. Seeking new, highly effective thermoelectrics. Science, 2020, 367: 1196–1197

33 Kajikawa T, Kimura N, Yokoyama T. Thermoelectric properties of intermetallic compounds: Mg_3Bi_2 and Mg_3Sb_2 for medium temperature range thermoelectric elements. In: Twenty-Second International Conference on Thermoelectrics. La Grande Motte, 2003. 305–308

34 Condron CL, Kauzlarich SM, Gascoin F, et al. Thermoelectric properties and microstructure of Mg_3Sb_2. J Solid State Chem, 2006, 179: 2252–2257

35 Bhardwaj A, Misra DK. Enhancing thermoelectric properties of a p-type Mg_3Sb_2-based Zintl phase compound by Pb substitution in the anionic framework. RSC Adv, 2014, 4: 34552–34560

36 Bhardwaj A, Chauhan NS, Misra DK. Significantly enhanced thermoelectric figure of merit of p-type Mg_3Sb_2-based Zintl phase compounds via nanostructuring and employing high energy mechanical milling coupled with spark plasma sintering. J Mater Chem A, 2015, 3: 10777–10786

37 Tamaki H, Sato HK, Kanno T. Isotropic conduction network and defect chemistry in $Mg_{3+\delta}Sb_2$-based layered Zintl compounds with high thermoelectric performance. Adv Mater, 2016, 28: 10182–10187

38 Zhang J, Song L, Pedersen SH, et al. Discovery of high-performance low-cost n-type Mg_3Sb_2-based thermoelectric materials with multi-valley conduction bands. Nat Commun, 2017, 8: 13901

39 Zhang J, Song L, Borup KA, et al. New insight on tuning electrical transport properties via chalcogen doping in n-type Mg_3Sb_2-based thermoelectric materials. Adv Energy Mater, 2018, 8: 1702776

40 Sun X, Li X, Yang J, et al. Achieving band convergence by tuning the bonding ionicity in n-type Mg_3Sb_2. J Comput Chem, 2019, 40: 1693–1700

41 Liu Z, Wang Y, Mao J, et al. Lithium doping to enhance thermoelectric performance of MgAgSb with weak electron-phonon coupling. Adv Energy Mater, 2016, 6: 1502269

42 Chen C, Li X, Li S, et al. Enhanced thermoelectric performance of p-type Mg_3Sb_2 by lithium doping and its tunability in an anionic framework. J Mater Sci, 2018, 53: 16001–16009

43 Mao J, Shuai J, Song S, et al. Manipulation of ionized impurity scattering for achieving high thermoelectric performance in n-type Mg_3Sb_2-based materials. Proc Natl Acad Sci USA, 2017, 114: 10548–10553

44 Shuai J, Mao J, Song S, et al. Tuning the carrier scattering mechanism to effectively improve the thermoelectric properties. Energy Environ Sci, 2017, 10: 799–807

45 Chen X, Wu H, Cui J, et al. Extraordinary thermoelectric performance in n-type manganese doped Mg_3Sb_2 Zintl: High band degeneracy, tuned carrier scattering mechanism and hierarchical microstructure. Nano Energy, 2018, 52: 246–255

46 Mao J, Wu Y, Song S, et al. Anomalous electrical conductivity of n-type Te-doped $Mg_{3.2}Sb_{1.5}Bi_{0.5}$. Mater Today Phys, 2017, 3: 1–6

47 Mao J, Wu Y, Song S, et al. Defect engineering for realizing high thermoelectric performance in n-Type Mg_3Sb_2-based materials. ACS Energy Lett, 2017, 2: 2245–2250

48 Imasato K, Kang SD, Ohno S, et al. Band engineering in Mg_3Sb_2 by

alloying with Mg_3Bi_2 for enhanced thermoelectric performance. Mater Horiz, 2018, 5: 59–64

49 Imasato K, Kang SD, Snyder GJ. Exceptional thermoelectric performance in $Mg_3Sb_{0.6}Bi_{1.4}$ for low-grade waste heat recovery. Energy Environ Sci, 2019, 12: 965–971

50 Kanno T, Tamaki H, Sato HK, et al. Enhancement of average thermoelectric figure of merit by increasing the grain-size of $Mg_{3.2}Sb_{1.5}Bi_{0.49}Te_{0.01}$. Appl Phys Lett, 2018, 112: 033903

51 Kuo JJ, Kang SD, Imasato K, et al. Grain boundary dominated charge transport in Mg_3Sb_2-based compounds. Energy Environ Sci, 2018, 11: 429–434

52 Shi X, Sun C, Bu Z, et al. Revelation of inherently high mobility enables Mg_3Sb_2 as a sustainable alternative to n-Bi_2Te_3 thermoelectrics. Adv Sci, 2019, 6: 1802286

53 Shi X, Zhao T, Zhang X, et al. Extraordinary n-type Mg_3SbBi thermoelectrics enabled by yttrium doping. Adv Mater, 2019, 31: 1903387

54 Wood M, Kuo JJ, Imasato K, et al. Improvement of low-temperature zT in a Mg_3Sb_2-Mg_3Bi_2 solid solution via Mg-vapor annealing. Adv Mater, 2019, 31: 1902337

55 Tritt T, Rowe D. Thermoelectrics Handbook: Macro to Nano. Boca Raton: CRC Press, 2005

56 Dresselhaus M , Chen G, Tang M , et al. New directions for low-dimensional thermoelectric materials. Adv Mater, 2007, 19: 1043–1053

57 Kauzlarich SM, Brown SR, Snyder GJ. Zintl phases for thermoelectric devices. Dalton Trans, 2007, 2099

58 Ohno S, Imasato K, Anand S, et al. Phase boundary mapping to obtain n-type Mg_3Sb_2-based thermoelectrics. Joule, 2018, 2: 141–154

59 Imasato K, Fu C, Pan Y, et al. Metallic n-type Mg_3Sb_2 single crystals demonstrate the absence of ionized impurity scattering and enhanced thermoelectric performance. Adv Mater, 2020, 32: 1908218

60 Delci Z, Shyamala D, Karuna S, et al. Enhancement of optical, thermal and hardness in KDP crystals by boron doping. Int J Chem Tech Res, 2012, 4: 816–826

61 Li HS, Qi YX, Gong JH, et al. High-pressure synthesis and characterization of thermal-stable boron-doped diamond single crystals. Int J Refractory Met Hard Mater, 2009, 27: 564–570

62 Yang S, Matejczyk DE, Determan W. High Temperature Stable Nanocrystalline SiGe Thermoelectric Material. U.S. Patent, 8,512,667. 2013-8-20

63 Imasato K, Ohno S, Kang SD, et al. Improving the thermoelectric performance in $Mg_{3+x}Sb_{1.5}Bi_{0.49}Te_{0.01}$ by reducing excess Mg. APL Mater, 2018, 6: 016106

64 Shuai J, Ge B, Mao J, et al. Significant role of Mg stoichiometry in designing high thermoelectric performance for $Mg_3(Sb,Bi)_2$-based n-type Zintls. J Am Chem Soc, 2018, 140: 1910–1915

65 Harman TC, Taylor PJ, Walsh MP, et al. Quantum dot superlattice thermoelectric materials and devices. Science, 2002, 297: 2229–2232

66 Yazawa K, Shakouri A. Optimization of power and efficiency of thermoelectric devices with asymmetric thermal contacts. J Appl Phys, 2012, 111: 024509

67 Yue SY, Zhang X, Stackhouse S, et al. Methodology for determining the electronic thermal conductivity of metals via direct nonequilibrium ab initio molecular dynamics. Phys Rev B, 2016, 94: 075149

68 Jørgensen LR, Zhang J, Zeuthen CB, et al. Thermal stability of

Mg$_3$Sb$_{1.475}$Bi$_{0.475}$Te$_{0.05}$ high performance n-type thermoelectric investigated through powder X-ray diffraction and pair distribution function analysis. J Mater Chem A, 2018, 6: 17171–17176

69 Murugasami R, Vivekanandhan P, Kumaran S, et al. Simultaneous enhancement in thermoelectric performance and mechanical stability of p-type SiGe alloy doped with Boron prepared by mechanical alloying and spark plasma sintering. J Alloys Compd, 2019, 773: 752–761

70 Chen B, Li J, Wu M, et al. Simultaneous enhancement of the thermoelectric and mechanical performance in one-step sintered n-type Bi$_2$Te$_3$-based alloys via a facile MgB$_2$ doping strategy. ACS Appl Mater Interfaces, 2019, 11: 45746–45754

71 Shu R, Zhou Y, Wang Q, et al. Mg$_{3+\delta}$Sb$_x$Bi$_{2-x}$ family: A promising substitute for the state-of-the-art n-type thermoelectric materials near room temperature. Adv Funct Mater, 2019, 29: 1807235

72 Song SW, Mao J, Bordelon M, et al. Joint effect of magnesium and yttrium on enhancing thermoelectric properties of n-type Zintl Mg^{3+}Y$_{0.02}$Sb$_{1.5}$Bi$_{0.5}$. Mater Today Phys, 2019, 8: 25–33

Author contributions   Chen X and Sui J designed the experiment. Chen X and Qu N conducted the sample synthesis and performance testing. Qin D, Xue W and Wang Y performed the microstructure characterization. Chen X, Guo f, and Zhu J wrote this article with support and guidance from Cai W, Zhang Q, and Sui J. All authors contributed to the general discussion.

Conflict of interest   The authors declare that they have no conflict of interest.

Supplementary information   Experimental details are available in the online version of the paper.

Xiaoxi Chen received his PhD degree in 2020 in materials science and engineering from Harbin Institute of Technology, China. His main research interests focus on the fabrication and properties of Zintl phase thermoelectric materials.

Jianbo Zhu is a PhD candidate in materials science and engineering at Harbin Institute of Technology. He received his BE degree from Harbin Institute of Technology in 2019. He mainly studies transport problems of electron and phonon using Boltzmann transport equation and first principles calculations.

Fengkai Guo is now a postdoctoral researcher at Harbin Institute of Technology, China. He received his doctorate in material science from Harbin Institute of Technology, China in 2020. His main research interests focus on the fabrication and properties of thermoelectric materials.

Jiehe Sui is currently a professor of material physics and chemistry at Harbin Institute of Technology. He received his PhD degree in materials science and engineering from Harbin Institute of Technology in 2006. After that, he spent two years as a visiting scholar at the University of Houston (2013–2015). His current research is mainly on thermoelectric materials and devices.

晶界散射与镁成分调控协同提高硼掺杂Mg$_3$Sb$_2$基材料的热电性能

陈晓曦[1†]，朱建博[1†]，秦丹丹[1]，曲诺[1]，薛文华[2]，王玉梅[2]，张倩[3]，蔡伟[1]，郭逢凯[1*]，隋解和[1*]

摘要   器件应用要求热电材料在服役温度范围内具有持续的高热电优值. 近年来，Zintl相化合物n-Mg$_3$Sb$_2$由于丰富的化学性质和结构复杂性而受到广泛关注，但是，n-Mg$_3$Sb$_2$难以在整个中温范围内保持良好的热电性能. 本文通过提高烧结温度，使合金平均晶粒尺寸增加了15倍，调控了晶界散射从而使载流子迁移率提高至180 cm^2 V^{-1} s^{-1}. 同时，更高的烧结温度优化了Mg成分以获得超低晶格热导率；采用硼掺杂获得了良好的热稳定性和更高的硬度. 电热输运特性的协同优化使得硼掺杂Mg$_3$Sb$_2$合金的热电性能在全温域提高明显，热电优值为0.62 (300 K)–1.81 (773 K)，在300–773 K之间的平均热电优值高达1.4，在热电器件应用方面极具潜力.